Organic Electronics 85 (2020) 105862

Contents lists available at ScienceDirect

Organic Electronics

journal homepage: http://www.elsevier.com/locate/orgel

Broadband-absorbing polycyclic aromatic hydrocarbon composite films on topologically complex substrates

David Bilger [a], Kwang-Won Park [a], Ali Abdel-Maksoud [b], Trisha L. Andrew [a,c,*]

[a] Department of Chemistry, University of Massachusetts Amherst, Amherst, MA, 01003, United States
[b] Department of Electrical Engineering, University of Massachusetts Amherst, Amherst, MA, 01003, United States
[c] Department of Chemical Engineering, University of Massachusetts Amherst, Amherst, MA, 01003, United States

ARTICLE INFO

Keywords:
Polycyclic aromatic hydrocarbon
Reactive vapor deposition
Fluoranthene
Downconversion
Textile electronics

ABSTRACT

Reactive vapor deposition (RVD) allows researchers to coat a diverse set of textiles with robust films of conjugated macromolecules and build conformally-integrated nanostructured electronics on textiles. However, the number of precursors amenable to RVD are limited, which in turn limits the variety of device architectures and optoelectronic functions that can be integrated with textile substrates. Here, we develop a dehydrogenative coupling reaction that can be used to create uniform, conformal and patternable polycyclic aromatic hydrocarbon (PAH) coatings on textiles using RVD protocols. PAHs possess large absorption coefficients, tunable band edges, high charge carrier mobilities and ambipolarity, meaning that a number of photonic and optoelectronic devices can be elaborated from the coatings reported here. We discuss, in particular, a fluoranthene/perifluoranthene composite PAH coating created using RVD, which exhibits strong light absorption over a large wavelength range and accompanying intermolecular energy transfer, qualifying it as a competitive photoactive material for conformally integrated, textile-based solar energy harvesters.

1. Introduction

Reactive vapor deposition (RVD) protocols employ mild vacuum (10^{-3} Torr) to deposit conformal and patternable films of conjugated macromolecules onto complex topographies [1,2]. By forcing vaporized reagents to converge over a surface, a chemical reaction (typically, an oxidative polymerization) and film growth occur concurrently. Due to the low temperatures and mild reactants used to effect this process, RVD is ideal for non-destructively integrating soft electronic materials with textiles and garments for various wearable applications, including energy storage [3], body heat harvesting [4] and personal thermal management [5]. Various sulfur heterocycles, such as thiophenes [1,6], 3, 4-ethylenedioxythiophene [2] and 1,3-dihydroisothianaphthene [7], and one metalloporphyrin [8] have been subjected to oxidative deposition using a small selection of custom-built reactors. However, we still need to demonstrate that constitutionally-complex monomers can be subjected to RVD protocols to form macromolecules with as much specificity and control as can be expected from traditional, solution-phase chemical synthesis methods. This endeavour is particularly necessary to develop a library of macromolecules with diverse and controllable optical and electronic properties, which are needed to integrate complex optoelectronic devices with flexible, non-planar substrates, such as woven or knit textiles.

As a starting point, we focus our efforts on a class of organic compounds called polycyclic aromatic hydrocarbons (PAHs), on account of their large absorption coefficients [9,10], tunable band edges [11], high charge carrier mobilities and ambipolarity [12,13]. PAHs display low solubility in a range of common solvents and are generally difficult to synthesize/purify at scale and process into large-area films [11]. A small selection of pyrolysis-based [14] and surface-assisted [15–17] techniques are used to synthesize PAHs in low (milligram) quantities for mechanistic and spectroscopic analysis. However, the specific demands of these processes (ultra-high vacuum and either pyrolytic conditions or oriented metal surfaces) disqualify them from being invoked for complex device fabrication, particularly on textile substrates.

Advantageously, PAHs are oxidizable and amenable to sublimation, meaning that they are perfect candidates for RVD. Here, we develop a strategy to form uniform, conformal PAH coatings on textiles using RVD protocols. The key to our strategy is to start with a hydrogenated precursor molecule—instead of the final, desired PAH repeat unit structure—to enable the oxidative chemical reaction at a reasonable temperature (< 250 °C) and pressure (10^{-3} Torr). Working specifically

* Corresponding author. Department of Chemistry, University of Massachusetts Amherst, Amherst, MA, 01003, United States.
E-mail address: tandrew@umass.edu (T.L. Andrew).

https://doi.org/10.1016/j.orgel.2020.105862
Received 27 April 2020; Received in revised form 25 May 2020; Accepted 7 June 2020
Available online 19 June 2020

with a hydrogenated fluoranthene precursor, we create a composite PAH coating that displays the added benefits of broadband absorption in the visible region (up to 660 nm) and efficient resonant energy transfer (downconversion) between its two main constituents. Broadband absorption and downconversion find relevance in a variety of nanophotonics applications, including bioimaging and photodynamic therapy [18], and are especially useful for simultaneously increasing the photoactive window of and minimizing thermalization losses in photovoltaics [19]. In sum, the work we present sets the stage for seamlessly adding photonic and photovoltaic functions to a wide range of commercial textiles.

2. Results and discussion

Cyclodehydrogenation is a versatile synthetic strategy to create PAHs and has been performed using electrochemical [20] and chemical [21] techniques. An exemplary precursor for these reactions is the fluoranthene molecule **2**, whose symmetrically reactive structure yields extended PAHs upon chemical [22] or electrochemical [23] cyclodehydrogenative coupling. However, volatilizing **2** requires impractically high temperatures (m.p. 403 °C) or ultra-low pressures (10^{-7} Torr) that inhibit reliable film formation when using RVD protocols. To address this problem, we posited that the more volatile, hydrogenated fluoranthene precursor, **1** [22,24], could undergo both cyclodehydrogenation and oxidative coupling during RVD (Fig. 1). Specifically, we hypothesized that exposure of **1** to $FeCl_3$ and heat would trigger both dehydrogenation at the *arylic* positions and coupling at the *peri* positions, thereby forming fluoranthene and perifluoranthene structures (**2** and **3**, respectively), as well as higher order PAHs.

Compound **1** remains an especially heavy monomer (MW = 480.188 g/mol) when compared to others commonly used in RVD (MW < 150 g/mol) [2]. Accordingly, we utilized a custom-built cylindrical quartz hot-wall reactor (Fig. 1) [1] with constricted path lengths to vaporize powders of **1** and $FeCl_3$. The reagents were arranged and heated in separate crucibles as depicted in Fig. 1, with the optimum substrate position determined through iterative experimentation (optimizing for large-area film coverage and uniformity). The crucible containing compound **1** was not heated beyond 250 °C to prevent thermal degradation (Fig. S1). Vapors of **1** and $FeCl_3$ were transported outside the heated regions using a small flow (< 2 sccm) of nitrogen gas, wherein a dark green film developed on the reactor walls. Substrates placed outside the heated region, including glass, silicon, ITO and various textiles, were fully coated by the dark green film. These coated substrates were then subjected to a 1:9 toluene:methanol rinse for 5 min to remove any remaining metal salts and by-products. Ultraviolet–visible (UV–vis) absorption spectroscopy showed the depletion of low-energy

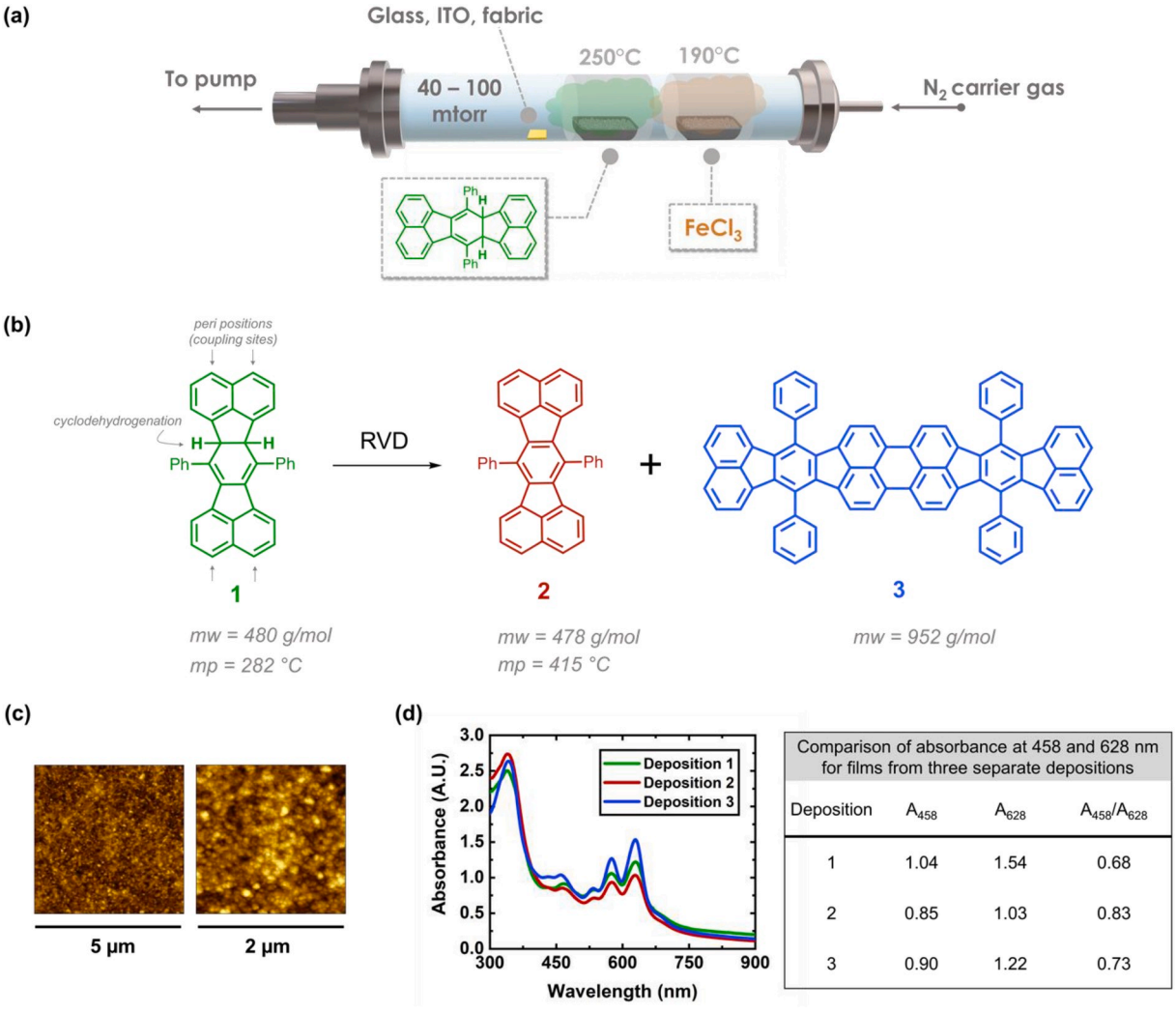

Fig. 1. (a) Hot-wall reactor and process conditions used to perform reactive vapor deposition (RVD) of polycyclic aromatic hydrocarbons (PAHs) using compound **1**. (b) Schematic of the cyclodehydrogenation and oxidative coupling reaction that takes place during this RVD process and the molecular structures of the two PAHs in the resulting film. (c) Topographical AFM images of RVD films on glass substrates after rinsing in alcohol to remove metal salts. (d) UV–vis absorption spectra of three separately deposited RVD films (left) and a table comparing their absorption values at 458 nm and 628 nm (right) to show batch-to-batch reproducibility.

absorption features with rinsing, likely corresponding to the quenching of radical cationic species (Fig. S2) formed during the oxidative deposition process. Further, analysis of the rinsed films using energy dispersive X-ray (EDX) spectroscopy confirmed that iron and chlorine were removed after rinsing (Fig. S2c).

Topographical images of the surface of rinsed RVD films, as acquired using atomic force microscopy (AFM), are provided in Fig. 1c. The images exhibit 100 nm sized clusters that are randomly distributed across the surface. X-ray diffraction spectra of the rinsed films only display peaks from the underlying substrate (Fig. S3), suggesting the films have an amorphous morphology, consistent with other phenyl-substituted perifluoranthenes [12,13]. The UV–Vis absorption spectra of three films taken from separate deposition batches display similar absorption profiles, which speaks to the remarkable batch-to-batch reproducibility of this RVD process (Fig. 1d, Table S1). For each sample, an absorption feature is observed at 330 nm, followed by a broad band between 400 and 500 nm and one vibronically-resolved band at higher wavelengths.

We found the absorption band between 400 and 500 nm particularly notable, given that *perifluoranthene* derivatives, such as **3**, do not display any absorbance features in this region. Based on its UV–vis absorption spectrum, we suspected that the RVD film was a composite and, indeed, thin-layer chromatography of partially-dissolved RVD samples revealed the presence of both a yellow and a blue-colored compound, which can be ascribed to the absorbance features at 458 nm and 628 nm, respectively (Fig. S4). The table in Fig. 1d compares the ratio of intensities at 458 nm and 628 nm observed for RVD films from three different depositions. The ratio of these absorbance intensities is largely invariant across different depositions, suggesting that this RVD process can reliably create composite films with consistent compound ratios.

Next, we attempted to dissolve the RVD films with an organic solvent to perform various spectroscopic characterizations for ascertaining chemical composition, and to compare their optical properties with those of well-defined control compounds synthesized following literature procedures (Fig. 2). Despite PAHs being weakly soluble in many common solvents, their absorption profiles can nonetheless be measured at very dilute concentrations due to their high oscillator strengths [12]. Therefore, even though we could not completely dissolve the RVD films, we isolated dilute solutions that were sufficient to record UV–vis absorption spectra, ^{1}H nuclear magnetic resonance (NMR) spectra and mass spectra. The solution UV–vis absorption spectra of dissolved RVD films resembled their solid-state equivalents, albeit with narrower band widths, slight hypsochromic shifts and more finely resolved spectral features. Using the solution and solid-state absorption spectra of chemically-synthesized compounds [22–24] as references, the two constituents (one yellow, one blue) of the composite RVD films could be tentatively assigned as compound **2** and compound **3**, respectively. Two signals at *m/z* values of 478 and 952 in the laser desorption ionization mass spectrum (LDI-MS, Fig. S5a) of the RVD films unambiguously confirmed these structure assignments. Lastly, the ^{1}H NMR spectrum of a dissolved RVD film (Fig. S5b) lacked any peaks in the vinylic region (between 5.0 and 5.5 ppm), indicating that compound **1** is absent. These characterization efforts collectively confirm that compound **1** undergoes both cyclodehydrogenation and oxidative coupling during RVD to create a composite film (an organic alloy) of compounds **2** and **3** that, together, create a broadband absorption profile in the visible region.

Interestingly, optical features arising from higher order, or extended, PAHs were not observed in RVD films, meaning that higher molecular weight species were not produced in notable quantities during the oxidative coupling process. To explain this observation, we turned to electronic structure calculations of **2** and **3** (Fig. S6). Previous semi-empirical calculations revealed that the highest occupied molecular orbital (HOMO) of **2** displays the largest orbital coefficients at the *peri* positions, meaning that coupling should primarily occur at these positions [25]. Our *ab initio* HF/6-31G calculations (Fig. S6) agree with these reports, which clarifies the reason we are able to exclusively isolate the dimeric perifluoranthene structure **3** without forming a mixture of constitutional isomers. Interestingly, the calculated HOMO of **3** reveals that the *peri* carbons have very small orbital coefficients—0.1034 in **3** vs 0.2779 in **2**—denoting that these accessible end sites do not contain sufficient electron density to produce PAH coupling products at reasonable rates. Only the carbon atoms in the bay and cove positions of **3** possess large enough orbital coefficients and sufficient electron

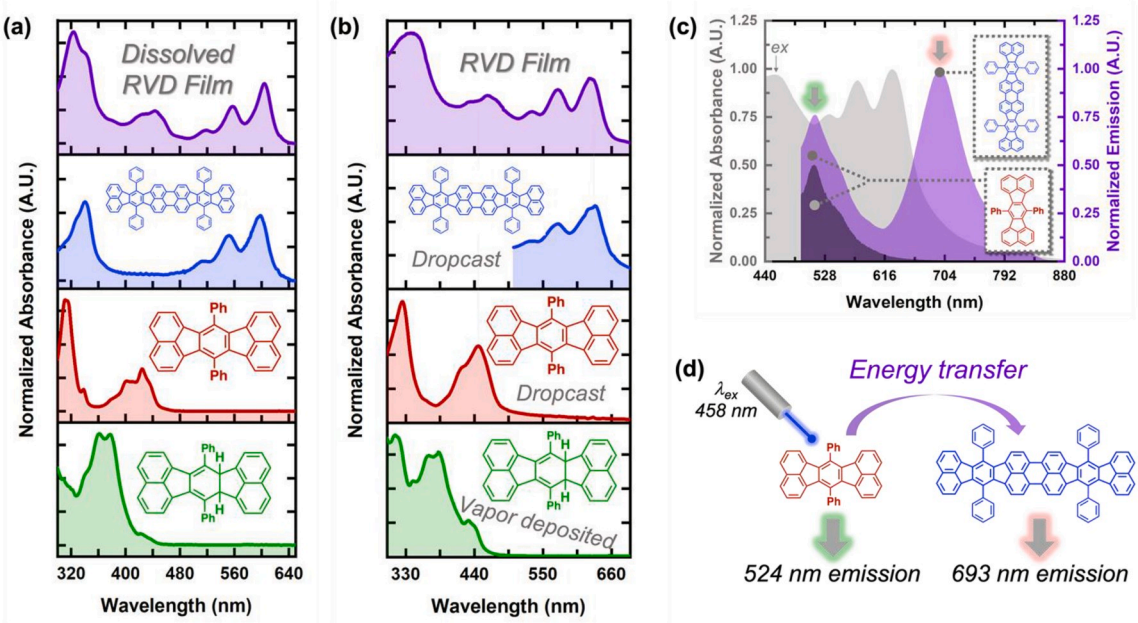

Fig. 2. (a) Solution-phase absorption spectra of compounds **1** (green), **2** (red), **3** (blue), and a partially-dissolved RVD film (purple). (b) Thin film absorption spectra of compounds **1** (green), **2** (red), **3** (blue), and an RVD film (purple). A valley was observed between 400 and 500 nm in the absorption spectrum of dropcast **3**. (c) Absorption (grey) and emission spectra (purple) of an RVD sample excited at 458 nm. The black curve is an emission spectrum of neat **2** (dropcast). (d) Illustration of energy transfer between **2** and **3** in an RVD film. (For interpretation of the references to color in this figure legend, the reader is referred to the Web version of this article.)

density to participate in oxidative coupling; however, these sites are too congested to form extended PAHs.

Emission spectra of the RVD films were recorded upon excitation at either 458 nm (the absorption maximum of compound **2**) or 628 nm (the absorption maximum of compound **3**). Two emission peaks arise when the RVD films are excited at 458 nm (Fig. 2 and S7): the first at λ_{em} 524 nm, identical to the emission spectrum of neat **2** (dropcast), and the second at λ_{em} 693 nm, identical in shape to the emission spectra of neat **3** [22]. No emission was observed when exciting thin films of neat **3** at 458 nm. Importantly, the emission peak at 693 nm is the only feature observed when the RVD films are excited at 628 nm. These observations indicate the presence of resonant energy transfer between compounds **2** and **3** in the composite RVD film. The calculated efficiency of resonant energy transfer from **2** to **3** in this composite film is 25% ± 10%, which is a reasonable efficiency considering that the RVD films are amorphous. Given the distance dependence of resonant energy transfer, which decays as R^6, we infer that compounds **2** and **3** must be separated by less than 100 nm from each other in the RVD films. This distance is comparable to the size of aggregates seen in our films using AFM imaging. The aggregates must, therefore, be composed of an intimate mixture of **2** and **3** to enable the observed resonance energy transfer, suggesting that **2** and **3** do not phase separate from one another during the RVD process or upon post-deposition rinsing. The uniformly well-mixed nature of this composite film is remarkable, as physical, electronic and excitonic coupling between components in a mixed molecular solid are hard to achieve [26].

To further confirm electronic coupling between **2** and **3** in the RVD films, the valence band spectrum and related secondary electron cutoff photoemission spectrum of the films were recorded on ITO using ultraviolet photoelectron spectroscopy (UPS, Fig. 3). The valence band spectrum provides a distribution of the condensed-phase binding energies (vs. vacuum level) of the occupied electronic states in a material. As a reference, a thin film (ca. 50 nm) of compound **2** was prepared via spincoating and its corresponding UPS spectrum was compared to that of the RVD films. The measured valence band edges of **2** (−5.86 eV) and the RVD films (−5.70 eV) are illustrated in Fig. 3b. The higher-lying valence band edge of our RVD samples supports the presence of electronic coupling between **2** and **3**, as interaction with the larger π-system of **3** should raise the valence band edge of the RVD films in relation to pristine films of **2**. For comparison, the valence band edges of perifluoranthenes with shorter conjugation compared to **3**, such as tetraphenyldibenzoperiflanthene (DBP), lie at ca. −5.5 eV [27]. The conduction band edges of **2** (−3.36 eV) and the RVD films (−3.88 eV) were calculated from their lowest energy absorption band edges. Because the RVD films are composed of both compounds **2** and **3**, with the lowest-energy absorption feature arising exclusively from the latter, the true conduction band of the composite films lies between −3.36 eV and −3.88 eV.

Patterned films were formed on both planar and non-planar surfaces using straightforward shadow-masking during RVD. Fig. 4a shows fluoranthene/perifluoranthene composite films patterned in the shape of a triangle and a rectangle following rinsing with 1:9 toluene:methanol to remove metal salts. Patterned films maintained well-defined edges after mask removal and solvent rinsing. Images of the same films are provided in Fig. 4b after a second solvent soak (25 min) in 1:9 toluene:hexane. The film color changes from a forest green to a grey-blue, indicating that the optical properties of the RVD films can be fine-tuned by deploying a second solvent soaking step. The table provided in Fig. 4c compares the raw absorbances of an RVD film at 458 nm and 628 nm as a function of

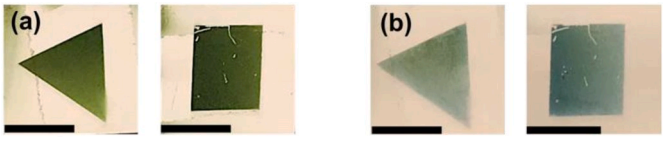

(c)

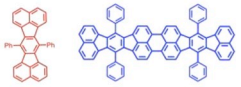

Washing time (min)	A_{458}	A_{628}	A_{458}/A_{628}
2	2.58	2.05	1.26
4	2.16	1.92	1.13
10	1.67	1.76	0.95
20	1.30	1.62	0.80

Fig. 4. Patterned PAH composite films grown on glass using RVD (a) before and (b) after soaking in 1:9 toluene:hexane to fine-tune color. (c) Table comparing the absorbance of an RVD film at 458 nm and 628 nm at different soaking times with 1:9 toluene:hexane. The black lines are 0.5 cm scale bars. (For interpretation of the references to color in this figure legend, the reader is referred to the Web version of this article.)

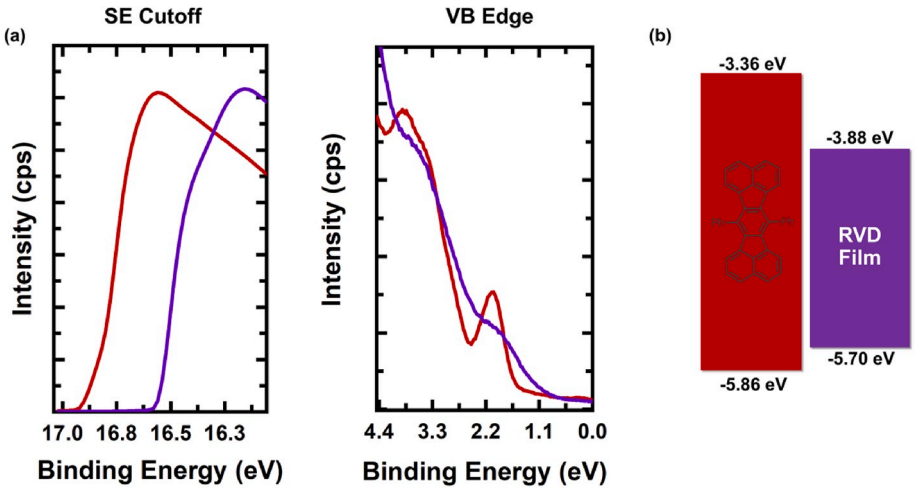

Fig. 3. (a) Representative secondary electron cutoff photoemission spectrum (left) and corresponding valence band spectrum (right) of a neat film of **2** (red) and an RVD film (purple), both on ITO. Both thin film samples were ca. 50 nm thick. (b) Illustration of the valence and conduction band edges of an RVD film and a neat film of **2**. (For interpretation of the references to color in this figure legend, the reader is referred to the Web version of this article.)

soaking time (corresponding spectra are provided in Fig. S8a). The absorbance at 458 nm decreases at a faster rate compared to that at 628 nm, suggesting that compound **2** is selectively removed from the RVD films with a toluene/hexane soak. Indeed, the absorption spectrum of the toluene/hexane bath in which the RVD films were soaked exactly matches the solution-phase absorption spectrum of pure **2** (Fig. S8b).

Linen swatches were also pattern coated with the same fluoranthene/perifluoranthene composite using RVD (Fig. 5a). Again, the RVD coating maintained well-defined edges on the prewoven linen substrates, even after the first solvent rinse to remove metal salts. The aforementioned toluene:hexane soaking step was also found to be effective for fine-tuning the final color of the RVD coating on linen: films change their apparent color from blue-green to blue after the toluene: hexane soak (Fig. 5b). Composite films were also deposited on conductive carbon cloth for imaging by scanning electron microscopy (SEM). Optical images of pristine carbon cloth depict a dark grey interwoven fabric (Fig. S9a), while SEM images of the uncoated samples reveal the striations of individual fibers (Fig. S9b). The carbon cloth substrates take on a visible green tint after being coated (Fig. S9c) and striations are no longer observed via SEM (Fig. 5c and S9d). These images reveal that the deposited PAH composite film wraps uniformly around the circumference of each individual fiber within the carbon cloth, which is an expected result due to the relatively high pressures (10^{-3} Torr) used during RVD. As a comparison, physical vapor deposition (PVD) of tetraphenyldibenzoperiflanthene (DBP) was performed under ultrahigh vacuum (10^{-7} Torr) on carbon cloth. SEM images of this film (Fig. 5d) reveal that large areas of the carbon cloth remain uncoated and that non-uniform aggregates of DBP are present over small regions of random fibers. These observations speak to the unique effectiveness of RVD as a processing technique for depositing uniform films of conjugated macromolecules on topographically complex substrates, such as textiles.

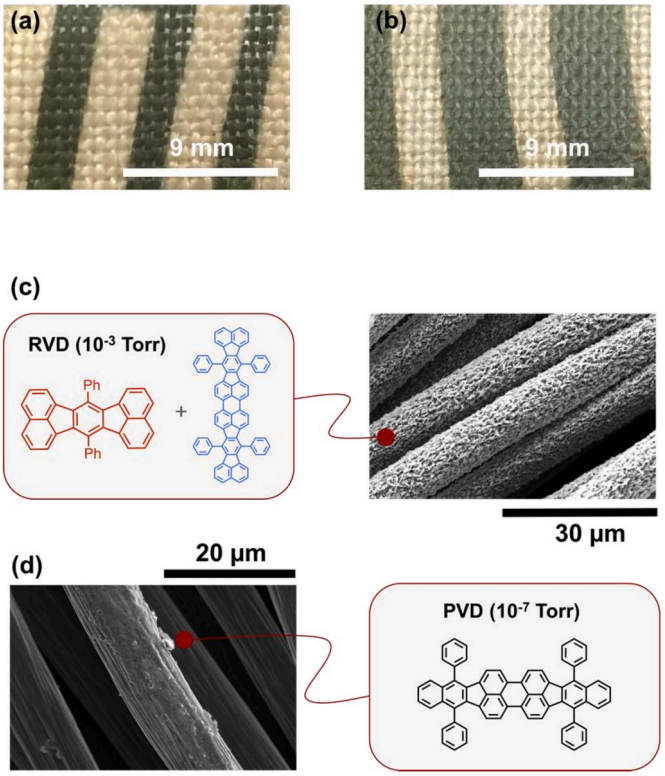

Fig. 5. Patterned PAH composite coatings on textiles. (a) PAH coating on linen and (b) the same linen swatch after soaking in 1:9 toluene:hexane to show color tunability. (c) SEM image of carbon cloth coated with a PAH composite using RVD. (d) SEM image of carbon cloth coated with the molecular semiconductor **DBP** using physical vapor deposition, showing irregular, nonuniform coverage. (For interpretation of the references to color in this figure legend, the reader is referred to the Web version of this article.)

3. Conclusions and future directions

We use a custom-built hot-wall reactor to enact a dehydrogenative coupling reaction that simultaneously synthesizes and deposits a composite PAH film onto topologically complex surfaces. The dehydrogenative coupling reaction is performed using reactive vapor deposition protocols and proceeds in a similar fashion, inside our reactor, as compared to solution-based precedents. Spectroscopic characterizations indicate that the films are a well-defined mixture of fluoranthene and perifluoranthene structures (compounds **2** and **3**), and electronic structure calculations suggest that molecular orbital densities limit the formation of higher order PAHs. Conformal and uniform coatings of this PAH composite can be created on textured and non-planar substrates, which is challenging to achieve with large or extended PAHs. Moreover, since the dehydrogenative coupling reaction is not substrate directed, thick and patternable films of these fluoranthene/perifluoranthene composites can be easily and reliably fabricated on any commercial textile. The composite films exhibit broadband and tuneable absorption of visible light (up to 660 nm), with compounds **2** and **3** also participating in resonant energy transfer to facilitate optical downconversion.

The unique attributes of the PAH composite film reported herein are thus: (1) They expand the repertoire of molecules amenable to RVD protocols. (2) They are patternable and conformal over inert, non-planar substrates, such as textiles. (3) Their optoelectronic properties, encompassing broadband absorption and resonance energy transfer (downconversion), make them attractive candidates for conformally integrated textile-based solar energy harvesters. Considering these advantageous features, work is currently being conducted in our laboratory to incorporate this composite PAH film into textile-based solar energy harvesters.

4. Experimental procedures

4.1. Materials

All solvents and reagents were purchased from Sigma Aldrich and used as received without further purification. 7,14-diphenylacenaphtho[1,2-k]-fluoranthene (**1**), 6a,14a-dihydro-7,14-diphenylacenaphtho[1,2-k]fluoranthene (**2**), and 4,4',7,7'-tetraphenyldiacenaphtho[1,2-k:1',2',k']diindeno[1,2,3-cd:1',2',3'-lm]-perylene (**3**) were synthesized following protocols reported by Müllen et al. [22].

4.2. Deposition protocols

Glass, ITO, and silicon substrates were cleaned using the following sequence prior to any depositions: (1) sonication in a detergent solution for 5 min, (2) Rinsing with DI water followed by additional sonication in acetone for 5 min, (3) immersion into boiling isopropanol for 5 min (2x), and (4) treatment with UV-ozone for 30 min.

Reactive vapor deposited samples were prepared by loading compound **1** and $FeCl_3$ into tungsten and ceramic crucibles, respectively. The distance between the crucibles and vacuum outlet/gas inlets of our reactor were kept consistent across all deposition batches. Substrates, including glass, ITO coated glass, silicon, linen fabric, and carbon cloth were taped onto PET and wrapped into a cylinder around the inner walls of the reactor and adjacent to the crucible containing **1**. The reactor was then pumped down with an Edwards direct-drive vacuum pump and maintained at pressures between 40 and 100 mTorr with a nitrogen gas inlet. Two resistive heating tapes were placed adjacent to each other and wrapped around regions of the reactor that contained **1** and $FeCl_3$. The substrates, while adjacent to **1**, were not within the heated region. The tape surrounding $FeCl_3$ was heated to 190 °C, while that surrounding **1**

was heated to 250 °C. The oxidant region began heating 2 min before the region containing **1** in order to maximize the intersectional area of both vapors. The length of the depositions, from when the oxidant region began heating to when the heating tapes were removed, lasted 20 min. In the case of samples prepared for ultraviolet photoelectron spectroscopy (UPS), the depositions were stopped after 15 min to yield thinner films. This type of RVD *protocol*, in which both reagent vapors intersect continuously and simultaneously throughout the deposition, is often referred to as *oxidative chemical vapor deposition*. The films were then washed for 20 min in 1:9 toluene:methanol followed by 10 min in 1:9 toluene:hexane, unless otherwise stated. RVD films fabricated over 20 min long depositions had film thicknesses of ca. 200 nm following washing.

Physical vapor transport of **1** was conducted using the aforementioned hot-wall reactor. However, oxidant was purposefully removed from the deposition, resulting in a yellow thin film of **1** as a control sample.

Physical vapor deposition (PVD) of tetraphenyldibenzoperiflanthene (DBP) was conducted in a commercial PVD chamber (Angstrom Nexdep, USA). DBP was placed in an aluminum crucible and loaded into the thermal evaporator. The sample was evaporated at a base pressure of 5 x 10^{-7} Torr. The films were deposited on carbon cloth at a rate of 0.3 Å/s up to a thickness of 250 nm, as monitored using an *in situ* quartz crystal microbalance.

4.3. Characterization

All thin films were prepared using RVD, unless otherwise noted. The thermal stability of **1** was determined using a TA Instruments thermal gravimetric analyzer (TGA) Q-500 at a ramp rate of 10 °C/min under nitrogen. Ultraviolet–Visible (UV–Vis) absorption spectra were collected using an Agilent 8453 spectrophotometer. Solution-based samples for absorption measurements were prepared by dissolving each compound in toluene at an appropriate concentration to yield a maximum absorption value below 1. Emission spectra of thin film samples were collected on a Horiba Jobin Yvon Fluorolog22 fluorimeter with an excitation wavelength specific to their absorption spectra. Mass spectra were acquired using an ultrafleXtreme MALDI-TOF mass spectrometer (Bruker Instruments, Billerica MA) equipped with a smartbeamTM laser at 355 nm. All samples were run without a matrix in reflectron mode. ^{1}H NMR spectra were obtained using a Bruker Avance 400 MHz nuclear magnetic resonance spectrometer. All measurements were taken in deuterated chloroform. UPS measurements were conducted using an Omicron SPHERA hemispherical analyzer with a He I light source (21.2 eV) and samples were prepared on ITO-coated glass.

Field-emission scanning electron microscopy (SEM) and energy-dispersive X-ray (EDX) spectroscopy were carried out using a Magellan 400 microscope. Thin film surfaces were also characterized using atomic force microscopy (AFM) (Veeco Dimension 3100, NY, USA). AFM images acquired under tapping mode were conducted with a PPP-NCHR cantilever (Force constant = 42 N/m, Nanosensors, Switzerland).

4.4. Calculations

Electronic structure calculations were performed using the Gaussian 09' software suite (HF/6-31G). Molecular structures were geometry optimized to a global minimum before molecular orbitals were calculated.

Author contributions

D.B. conceptualized and performed experiments, analyzed data and wrote the manuscript. K.-W.P. performed experiments and analyzed data. A.A.-M. performed experiments. T.L.A. designed and conceptualized the study, analyzed data, raised funds and wrote the manuscript.

Declaration of competing interest

The authors declare that they have no known competing financial interests or personal relationships that could have appeared to influence the work reported in this paper.

CRediT authorship contribution statement

David Bilger: Methodology, Formal analysis, Investigation, Writing - original draft, Visualization. **Kwang-Won Park:** Formal analysis, Investigation, Writing - review & editing. **Ali Abdel-Maksoud:** Validation, Investigation. **Trisha L. Andrew:** Conceptualization, Methodology, Writing - review & editing, Supervision, Funding acquisition.

Acknowledgements

This work is supported by the National Science Foundation under CHEM MSN 1807743. Mass spectroscopy data were obtained at the University of Massachusetts Mass Spectrometry Center. The authors thank Babgen Manookian and Professor Scott M. Auerbach for their assistance with electronic structure calculations.

Appendix A. Supplementary data

Supplementary data to this article can be found online at https://doi.org/10.1016/j.orgel.2020.105862.

References

[1] N. Cheng, L. Zhang, J.J. Kim, T.L. Andrew, Vapor phase organic chemistry to deposit conjugated polymer films on arbitrary substrates, J. Mater. Chem. C. 5 (2017) 5787–5796.
[2] D. Bilger, S.Z. Homayounfar, T.L. Andrew, A critical review of reactive vapor deposition for conjugated polymer synthesis, J. Mater. Chem. C. 7 (2019) 7159–7174.
[3] L. Zhang, W. Viola, T.L. Andrew, High energy density, super-deformable, garment-integrated microsupercapacitors for powering wearable electronics, ACS Appl. Mater. Interfaces 10 (2018) 36834–36840.
[4] L.K. Allison, T.L. Andrew, A wearable all-fabric thermoelectric generator, Adv. Mater. Technol. (2019), 1800615.
[5] L. Zhang, M. Baima, T.L. Andrew, Transforming commercial textiles and threads into sewable and weavable electric heaters, ACS Appl. Mater. Interfaces 9 (2017) 32299–32307.
[6] D.C. Borrelli, S. Lee, K.K. Gleason, Optoelectronic properties of polythiophene thin films and organic TFTs fabricated by oxidative chemical vapor deposition, J. Mater. Chem. C. 2 (2014) 7223–7231.
[7] D.C. Borrelli, K.K. Gleason, Tunable low bandgap polyisothianaphthene via oxidative chemical vapor deposition, Macromolecules 46 (2013) 6169–6176.
[8] G. Bengasi, K. Baba, G. Frache, J. Desport, P. Gratia, K. Heinze, N.D. Boscher, Conductive fused porphyrin Tapes on sensitive substrates by a chemical vapor deposition approach, Angew. Chem. Int. Ed. 58 (2018) 2103–2108.
[9] Z. Wang, A. Meijerink, Dye-sensitized downconversion, J. Phys. Chem. Lett. 9 (2018) 1522–1526.
[10] R. Rieger, K. Müllen, Forever young: polycylic aromatic hydrocarbons as model cases for structural and optical studies, J. Phys. Org. Chem. 23 (2010) 315–325.
[11] X.Y. Wang, X. Yao, K. Müllen, Polycylic aromatic hydrocarbons in the graphene era, Sci. China Chem. 62 (2019) 1099–1144.
[12] A.N. Bartynski, S. Grob, T. Linderl, M. Gruber, W. Brütting, M.E. Thompson, Organic solar cells with open circuit voltage over 1.25 V employing tetraphenyldibennnzoperiflanthene as the acceptor, J. Phys. Chem. C 120 (2016) 19027–19034.
[13] Y. Li, R.G. Clevenger, L. Jin, K.V. Kilway, Z. Peng, Spin-coated thin films of polycyclic aromatic hydrocarbons exhibiting high SCLC hole mobilities, J. Phys. Chem. C 120 (2016) 841–852.
[14] V.M. Tsefrikas, L.T. Scott, Geodesic polyarenes by flash vacuum pyrolysis, Chem. Rev. 106 (2006) 4868–4884.
[15] S. Clair, D.G. de Oteyza, Controlling a chemical coupling reaction on a surface: tools and strategies for on-surface synthesis, Chem. Rev. 119 (2019) 4717–4776. \.
[16] C. Sanchez-Sanchez, J.I. Martinez, N.R. del Arbol, P. Ruffieux, R. Fasel, M.F. Lopez, P.L. de Andres, J.A. Martin-Gago, On-surface hydrogen-induced covalent coupling of polycyclic aromatic hydrocarbons via a superhydrogenated intermediate, J. Am. Chem. Soc. 141 (2019) 3550–3557.
[17] M. Di Giovannantonio, J.I. Urgel, U. Beser, A.V. Yakutovich, J. Wilhelm, C. A. Pignedoli, P. Ruffieux, A. Narita, K. Müllen, R. Fasel, On-surface synthesis of indenofluorene polymers by oxidative five-membered ring formation, J. Am. Chem. Soc. 140 (2018) 3532–3536.

[18] C. Chen, Y. Chunhui Yang, P.N. Prasad, Nanophotonics and nanochemistry: controlling the excitation dynamics for frequency up- and down- conversion in lanthanide-doped nanoparticles, Acc. Chem. Res. 46 (2013) 1474–1486.
[19] W.A. Tisdale, K.J. Williams, B.A. Timp, D.J. Norris, E.S. Aydil, X.-Y. Zhu, Hot-electron transfer from semiconductor nanocrystals, Science 328 (2010) 1543–1547.
[20] J.D. Debad, J.C. Morris, V. Lynch, P. Magnus, A.J. Bard, Dibenzotetraphenylperiflanthene: synthesis, photophysical properties, and electrogenerated chemiluminescence, J. Am. Chem. Soc. 118 (1996) 2374–2379.
[21] X. Zhang, Z. Xu, W. Si, K. Oniwa, M. Bao, Y. Yamamoto, T. Jin, Synthesis of extended polycyclic aromatic hydrocarbon by oxidative tandem spirocyclization and 1,2-aryl migration, Nat. Commun. 8 (2017) 15073.
[22] M. Wehmeier, M. Wagner, K. Müllen, Novel perylene chromophores obtained by a facile oxidative cyclodehydrogenation route, Chem. Eur J. 7 (2001) 2197–2205.
[23] J.D. Debad, A.J. Bard, Electropolymerization of acennaph-tho[1,2-k]fluoranthene derivatives: formation of a new conductive electroactive electrochromic hydrocarbon ladder polymer, J. Am. Chem. Soc. 120 (1998) 2476–2477.
[24] Y.T. Wu, T. Hayama, K.K. Baldridge, A. Linden, J.S. Siegel, Synthesis of fluoranthenes and indenocorannulenes: elucidation of chiral stereoisomers on the basis of static molecular bowls, J. Am. Chem. Soc. 128 (2006) 6870–6884.
[25] B.F. Plummer, L.K. Steffen, T.L. Braley, W.G. Reese, K. Zych, G. Van Dyke, B. Tulley, Study of the geometry effects on heavy atom perturbation of the electronic properties of derivatives of the non-alternate polycyclic aromatic hydrocarbons fluoranthene and acenaphtho[1,2-k]fluoranthene, J. Am. Chem. Soc. 115 (1993) 11542–11551.
[26] X. Huang, X. Liu, K. Ding, S.R. Forrest, Is there such a thing as a molecular organic alloy? Mater. Horiz. 7 (2019) 244–251.
[27] Y. Peng, L. Zhang, T.L. Andrew, High open-circuit voltage, high fill factor single-junction organic solar cells, Appl. Phys. Lett. 105 (2014), 083304.